Arabian Journal for Science and Engineering
https://doi.org/10.1007/s13369-025-10937-w

RESEARCH ARTICLE-CHEMISTRY

g-C_3N_4@Fe_3O_4 Nanomaterial Synthesis for Magnetic Solid-Phase Extraction and Photocatalytic Removal of Basic Blue 3

Nebiye Kizil[1,2,3] · Nilgun Kayaci[4] · Duygu Erkmen Erbilgin[2] · Mehmet Lütfi Yola[5] · Erkan Yilmaz[6,7] · Mustafa Soylak[8,9,10]

Received: 11 June 2025 / Accepted: 27 November 2025

Abstract

The present research synthesized a g-C_3N_4@Fe_3O_4 hybrid material for efficient magnetic solid-phase extraction (MSPE) and photocatalytic degradation of Basic Blue 3 (BB3) dye from wastewater. Characterization of the synthesized g-C_3N_4@Fe_3O_4 was conducted through Fourier transform infrared spectroscopy (FTIR), X-ray diffraction (XRD), scanning electron microscopy (SEM), and energy-dispersive X-ray spectroscopy (EDX). The optimization of the method was carried out by examining parameters such as pH, g-C_3N_4@Fe_3O_4 amount, sample volume, and adsorption/desorption duration. In addition, analytical performance criteria such as limit of detection (LOD), limit of quantification (LOQ), and relative standard deviation (RSD) of the MSPE method were calculated as 1.29 $\mu g\ L^{-1}$, 4.28 $\mu g\ L^{-1}$, and 1.9%, respectively. The method was applied to real samples, including wastewater and textiles, and validated through addition/recovery studies for the magnetic solid-phase extraction procedure. The recoveries were gained between 91 and 100%. The reusability synthesized g-C_3N_4@Fe_3O_4 was also evaluated. The recoveries for Basic Blue 3 dye decreased to 81% after the fourth experiment. Furthermore, the photocatalytic performance of the g-C_3N_4@Fe_3O_4 hybrid material was evaluated due to its good surface area and strong interaction with Basic Blue 3 dye. The photocatalytic activity of g-C_3N_4@Fe_3O_4 hybrid material was calculated as 96.8% for 100 mg in 300 min.

Keywords Basic Blue 3 · spectrophotometry · Magnetic solid-phase extraction · Photocatalytic degradation · Green chemistry · g-C_3N_4@Fe_3O_4

1 Introduction

Dyes can be defined as synthetic or natural compounds that, when applied to any substance, temporarily change its crystal structure, resulting in the coloration of that substance. Dyes are stable, aromatic molecules that are difficult to degrade [1–4]. These are divided into groups such as acid, azo, and nitro dyes, indigo, disperse, diarylmethane, and phthalocyanine reactive, disperse, basic, metal complex, and sulfur dyes, whose physical and chemical structures are very different and diverse [1, 2, 5–7].

One of the textile dyes Basic Blue 3 (BB3) dye, a type of basic synthetic dye, is used to color products such as fabrics, acrylic fibers, and textiles. These dyes are widely used in the textile industry because they do not fade, have a vivid and

✉ Mustafa Soylak
soylak@erciyes.edu.tr

1 Faculty of Engineering, Department of Basic Sciences, Hasan Kalyoncu University, Gaziantep, Turkey

2 Environmental Application and Research Center, Hasan Kalyoncu University, Gaziantep, Turkey

3 Environmental Science and Energy Management Program, Hasan Kalyoncu University, Gaziantep, Turkey

4 Department of Materials Science and Nanotechnology Engineering, Abdullah Gul University, Kayseri 38080, Turkey

5 Faculty of Health Sciences, Department of Nutrition and Dietetics, Hasan Kalyoncu University, Gaziantep, Turkey

6 Department of Analytical Chemistry, Faculty of Pharmacy, Erciyes University, Kayseri, Turkey

7 Nanotechnology Research Center (ERNAM), Erciyes University, Kayseri, Turkey

8 Department of Chemistry, Faculty of Sciences, Erciyes University, Kayseri 38039, Turkey

9 Technology Research and Application Center (TAUM), Erciyes University, Kayseri, Turkey

10 Turkish Academy of Sciences (TUBA), Cankaya, Turkey

Published online: 16 December 2025

intense color, and are lightfast. They are commonly used to color wool, silk, linen, cotton, and fabrics. In addition, BB3 dye, a toxic reactive dye, can cause some diseases in the human body, such as eyes and skin problems [8, 9].

The majority of synthetic dyes are mostly used in the textile industry. In these organizations, the excessive use of drinking water and also the generation of dye-containing wastewater during production (dyeing) processes such as washing, bleaching, and dyeing are the issues that are of most concern. Color pollution caused by textile dyes not only damages the aesthetic appearance of water but also prevents the interaction of water and light. So, the rate of photosynthesis and oxygen content in water are reduced and biological vitality is damaged [10–13]. As a result, pollution of industrial wastewater by such organic and inorganic compounds causes serious environmental problems due to their toxic and mutagenic effects on both humans and other organisms living in water and soil [14, 15]. That is why, researchers have been working on the improvement of wastewater.

Since textile dyes contain amine and azo groups and are highly durable, they are difficult to separate them from the wastewater by conventional methods [10, 16]. For this reason, physical (adsorption, nanoparticle utilization, filtration, ion-exchange, and oxidation) chemical (coagulation/flocculation, ozonation), biological (biodegradation/bioremediation), and combinatorial treatment processes are utilized [9, 17–19]. In this paper, an adsorption technique has been developed to separate and analysis of textile dye.

Adsorption is a low-cost and rapid physical process by which an analyte is rapidly and efficiently taken up from wastewater onto the surface of a solid adsorbent. The principle of the solid-phase extraction (SPE) method is found on the adsorption technique. Typical adsorbent materials are zeolite, silica gel, activated carbon, graphene oxide, carbon nanotubes, and graphite [20–22].

The g-C_3N_4, a two-dimensional conjugated polymer containing carbon and nitrogen, is generally synthesized by processes such as sol-gel and thermal polymerization method with cyanimide, thiourea, dicyandiamide, and melamine. The g-C_3N_4 has been widely used due to its outstanding properties such as low cost, easy availability and synthesis, metal-free, large surface area, fast electron transfer π–π conjugation structure, excellent visible light focusing and polymeric semiconductor, biocompatibility. Due to these superior properties, g-C_3N_4 is mostly utilized in applications such as fuel cells, heavy metals, organic pollutants, biosensors, gas, and drug determination [23–25]. In addition to the separation, enrichment, determination of organic or inorganic species processes, catalytic studies have been carried out for photocatalytic removal of the analyte from wastewater [26–29].

Photocatalytic degradation reactions are based on the principle that the degradation reactions, which take place in nature for a long time, are degraded in shorter times with the help of light and a photocatalyst. Organic water pollutants such as methylene blue, rhodamine B etc., and inorganic pollutants such as chromium can be eliminated from the environment by photocatalytic degradation reactions [30–32]. In these reactions, the photocatalysts play a very active role in reducing the duration of the degradation reactions together with UV light. The most commonly used photocatalysts are TiO_2 and ZnO semiconductors [33–35]. In addition to these, many catalysts such as g-C_3N_4, ZnS and Fe_3O_4 are used as photocatalysts. While the effect of each of them is different when used separately, highly effective photocatalysts have been obtained with nanocomposites formed by their synthesis together [36–38]. Along with TiO_2, ZnO and magnetic nanoparticles, two-dimensional materials, carbon nanotubes, graphene/graphene oxide, nanodiamonds, metal organic framework (MOF) and nanocomposites containing them are quite prominent as photocatalysts in the literature [39–42]. Even some materials with low catalytic activity can be modified into nanocomposites to obtain photocatalysts with high activity. Photocatalytic activity has been increased with multiple nanomaterials that come together with different superior properties such as the width of the surface area and the width/narrowness of the electron band gap [43–46].

In solid-phase extraction and photocatalytic removal studies, the ability to use the same material multiple times is important in terms of developing low-cost, environmentally friendly, processes that generate minimum process waste. From this point of view, the use of magnetic materials in both solid-phase extraction and photocatalytic applications, with the help of an externally applied magnetic field, allows the magnetic materials to be separated from the solution medium and used repeatedly, which is an important solution. For these reasons, the high adsorption and photocatalytic performance of g-C_3N_4 nanomaterial were combined with the magnetic properties of Fe_3O_4 nanoparticles in this study.

This paper is the first to investigate both magnetic solid-phase extraction (MSPE) and photocatalytic degradation of BB3 dye. For this, g-C_3N_4@Fe_3O_4 hybrid material was synthesized for usage in these processes. Furthermore, the magnetic solid-phase extraction (MSPE) method performance of the adsorbent for the separation and also preconcentration of BB3 dye from real samples were evaluated. The successfully optimized method was implemented to textiles, drinking water and wastewater samples.

2 Experimental

2.1 Instrumentation and Reagents

The BB3 dye stock solution, the buffer solutions, and the solutions of the components whose matrix effect was studied were prepared using an ultrasonic bath (Selectra, Spain) or a vortex mixer (Thermomac, Turkiye). The target analyte was analyzed by UV–Vis spectrometry (PerkinElmer Lambada 25; Norwalk, CT, USA). In addition, pH measurements were performed during all optimization steps and real sample extraction studies using a Hanna HI 2211 pH meter (Hanna, USA). Finally, a Nuve Water Distiller ND-4 was employed to produce distilled water for use in the experimental procedures. Furthermore, muffle furnace (Optic İvymen System/Lithuanıa), magnetic stirrer (Velp Scientifica, Italy), and oven (Nüve FN 500) were used for material synthesis.

All chemicals used in the MSPE technique for extraction of BB3 dye were analytical purity. Urea (Isolab/Germany), ethylene glycol (Carlo Erba/France), iron (III) chloride hexahydrate ($FeCl_3$) (Sigma-Aldrich, USA) were utilized to synthesis nanomaterials and also design methods.

2.2 Synthesis g-C_3N_4@Fe_3O_4 Nanomaterial

For the separation/enrichment of BB3 dye by MSPE method, graphitic carbon nitride synthesis was first carried out. For this, g-C_3N_4 nanoparticles (NPs) were obtained by calcination method, which is a simple and fast method. Then, magnetic properties were imparted to this material in order to prevent material loss and complete separation. To achieve this, 1.0 g of urea powder was transferred to a porcelain crucible and subjected to heating in a muffle furnace at a temperature of 550 °C for approximately 4 h. After calcination, the NPs were cooled at room temperature. The yellowish-colored g-C_3N_4 NPs obtained were weighed 0.5 g and placed in a beaker. 20 mL ethylene glycol was added and left in an ultrasonic bath for 20 s. In another beaker, 0.5 g $FeCl_3$, 2 g CH_3COONa, and 15 mL ethylene glycol were added. These mixtures were then combined and stirred in a magnetic stirrer until homogeneous. The mixture was transferred to a Teflon unit, and solvothermal treatment was carried out at 200 °C for 12 h. The formed g-g-C_3N_4@Fe_3O_4 NPs were collected with the help of a neodymium magnet and removed from the aqueous phase. Finally, impurities were removed by washing with ethanol and distilled water and dried at 80 °C [36, 47, 48].

2.3 Degradation of BB3 Dye

The photocatalytic performance of g-C_3N_4@Fe_3O_4 nanocomposite was determined using a 150 mL aqueous model solution of 10 ppm BB3 dye. In total,100 mg g-C_3N_4@Fe_3O_4 nanocomposite material was added to the dye solution and stirred overnight in the dark using a magnetic stirrer set at 1000 rpm. This ensured that the g-C_3N_4@Fe_3O_4 nanocomposite absorbed all the dye it could absorb. The final mixture was placed in a continuously stirred photocatalytic system with a 400 W UV halogen lamp (365 nm wavelength). The mixture was periodically sampled every 30 min, and the dye degradation versus time was analyzed by UV–Vis spectrophotometer. The dye degradation observed here was calculated according to the given equation.

$$\deg(\%) = \frac{C_0 - C_t}{C_t} \times 100$$

where C_0 (mg/mL) is the initial concentration of BB3 dye at 655 nm and C_t (mg/mL) is the concentration of BB3 dye at a given time "t" min. Since the degradation kinetics of BB3 dye fits the Langmuir–Hinshelwood (LH) model, it was found using the Langmuir-Hinshelwood (LH) kinetic model. The observation of a linear relationship during degradation confirmed that it follows the LH model.

$$\mathrm{In}\left\{\frac{C_0}{C_t}\right\} = -kt$$

where C_0, C_t, k and t are initial concentrations of BB3 dye, the concentration of BB3 dye at 655 nm at given time "t" min, kinetic constant and time, respectively.

$$\mathrm{In}\ 2 = kt_{1/2} = 0.693$$

where $t_{1/2}$ is the half-life time. It is defined as the time it taken for the initial concentration of the analyte to reach half [36, 49–51].

2.4 MSPE Methodology

The model solutions, incorporating components BB3 dye, were formulated using a total sample volume of 10 mL. Initially, the pH values of the solutions have been adjusted to 8 using a buffer solution (NaH_2PO_4/Na_2HPO_4). Subsequently, 10 mg of g-C_3N_4@Fe_3O_4 nanoparticles were added to these solutions, and the mixture was stirred for a duration of 3 min via vortex to adsorption of BB3 dye molecules on the adsorbent. Finally, the adsorbent was separated from the sample solutions through its magnetic property. The dye was then removed from the adsorbent surface by decanting with ethanol. These mixtures were blended for 4 min, in order to desorption studies. The extraction phase including BB3 was analyzed using a spectrophotometer at 655 nm [52].

2.5 MSPE-Based Sample Preparation

The developed MSPE method was implemented to fibers and wastewater samples. For this, 1 g of the fibers to be analyzed for BB3 dye weighed, and ethanol was added to them. The resulting mixtures were left in an ultrasonic bath for about 1 h. The optimized MSPE method was applied by taking 200 μL of BB3 dye, which completely passed from the fibers to the liquid phase. Furthermore, the wastewaters were passed through a 0.22 μm filter and kept at 4 °C prior to analysis using the MSPE technique with g-C_3N_4@Fe_3O_4 nanomaterials. As a result, the BB3 dye in these samples was measured using a UV–Vis spectrophotometer.

3 Results and Discussion

3.1 Characterization of g-C_3N_4@Fe_3O_4 Nanocomposite

XRD spectrum of Fe_3O_4 NPs exhibits diffraction peaks at $2\theta = 31.0$, 35.1, 42.7, 53.6, and 57.2°, which correspond to the planes of (220), (311), (400), (422), and (511), respectively, of the magnetite Fe_3O_4 NP phase (JCPDS Card No. 01-075-0449). A peak at $2\theta = 13.04$ (100) and 27.02° (002) is observed, which can be attributed to graphitic planes of g-C_3N_4 NPs (JCPDS 87–1526) (Fig. 1a) [53, 54]. The average crystal size of the g-C_3N_4@Fe_3O_4 nanocomposite was calculated as 74.38 nm using the Scherrer equation.

As depicted in Fig. 1b, the FTIR spectrum exhibits a broad peak around 3200 cm^{-1}, which can be attributed to the presence of adsorbed H_2O molecules, as well as terminal NH_2 or N–H groups located at defect sites within the aromatic ring. This peak is indicative of N–H asymmetric stretching vibrations. The multiple absorption bands observed in the 1200–1650 cm^{-1} range correspond to characteristic stretching modes of the C–N aromatic repeat unit, as well as C–N and C=N bond stretching vibrations, which are typical of triazine/s-triazine aromatic rings. Furthermore, the absorption band at approximately 806 cm^{-1} is associated with the out-of-plane bending vibrations inherent to these aromatic rings. The medium-intensity peak at 533 cm^{-1} is attributed to Fe–O stretching vibrations (Fig. 1b, Table S1) [36].

The UV–Vis spectra were observed for g-C_3N_4, Fe_3O_4, and hybrid g-C_3N_4@Fe_3O_4 NPs (Fig. S1). It was determined that g-C_3N_4 and Fe_3O_4 had maximum absorption at wavelengths compatible with the literature [55]. In addition, it was determined that the wavelength absorption peaks of g-C_3N_4@Fe_3O_4 NPs belonged to both nanomaterials.

SEM images of Fe_3O_4, g-C_3N_4, and hybrid g-C_3N_4@Fe_3O_4 NPs are shown in Fig. 2. The Fe_3O_4 NPs are shown in Fig. 2a, and the layered structure in graphite resulting from the weak Van der Waals interaction is shown in Fig. 2b. It can be understood from the SEM image of g-C_3N_4@Fe_3O_4 NPs that Fe_3O_4 NPs are spherically distributed on the surface of g-C_3N_4 (Fig. 2c) [56]. The SEM-EDX spectra obtained in Fig. 3a show that the weight percentages of C, N, and O in g-C_3N_4 NPs are 31.37, 64.04, and 4.59. In addition, the weight percentages of C, N, O, Fe for synthesized g-C_3N_4@Fe_3O_4 NPs were obtained as 10.19, 10.12, 29.49, 50.2, respectively (Fig. 3b).

3.2 The BB3 Dye Degradation

Many nanomaterials have been developed as an alternative to the photocatalysts most used in photocatalytic reactions. g-C_3N_4 nanomaterial is a material with a very large surface area and adsorption capacity. Therefore, it has been suggested that it can be a good photocatalyst [47, 48, 50]. To increase the photocatalytic activity of g-C_3N_4, we synthesized an alternative nanocomposite to the existing photocatalysts by combining it with Fe_3O_4 magnetic nanomaterial and investigated its effect on photocatalytic degradation in different photocatalyst amounts. When the photocatalytic degradation of g-C_3N_4 on BB3 dye organic dye was investigated, it was determined that it degraded around 76.6% of the dye after 300 min (Fig. 4b).

The adsorption capacity of g-C_3N_4 is also very effective in this reaction. When the photocatalytic activity of Fe_3O_4 alone was investigated, it was determined as 6.5% after 300 min. In examining the photocatalytic degradation performance of the g-C_3N_4@Fe_3O_4 nanocomposite obtained by combining these two materials, the determination of the amount of the photocatalyst was first investigated. To determine the optimum amount of photocatalyst, the degradation of BB3 dye was monitored for 300 min with 50, 100, and 150 mg g-C_3N_4@Fe_3O_4 photocatalyst amounts. As a result of 300 min photocatalytic degradation reaction, 92.73, 96.88 and 86.34% were obtained for 50, 100, and 150 mg photocatalysts, respectively (Fig. 4b). In the light of these data, the optimum amount of photocatalyst was determined as 100 mg (Fig. 4a). The percentage of dye degradation observed with 50 mg of catalyst is due to the low amount of catalyst. In addition, it can be said that the low degradation observed at 150 mg of photocatalyst is due to the decrease in the penetration of UV light in the solution environment as a result of the excess amount of photocatalyst [57, 58].

The reaction kinetics were evaluated for varying amounts of g-C_3N_4@Fe_3O_4 photocatalyst, and a linear regression analysis was performed, yielding a slope corresponding to the first-order rate constants derived from the $\ln(C_0/C_t)$ plots as a function of time (Fig. 5a). Likewise, the reaction half-life-time ($t_{1/2}$) and rate constants (K) were also calculated for different amounts of g-C_3N_4@Fe_3O_4 photocatalyst (Fig. 5b). The nanomaterials rate values were determined as 0.004609,

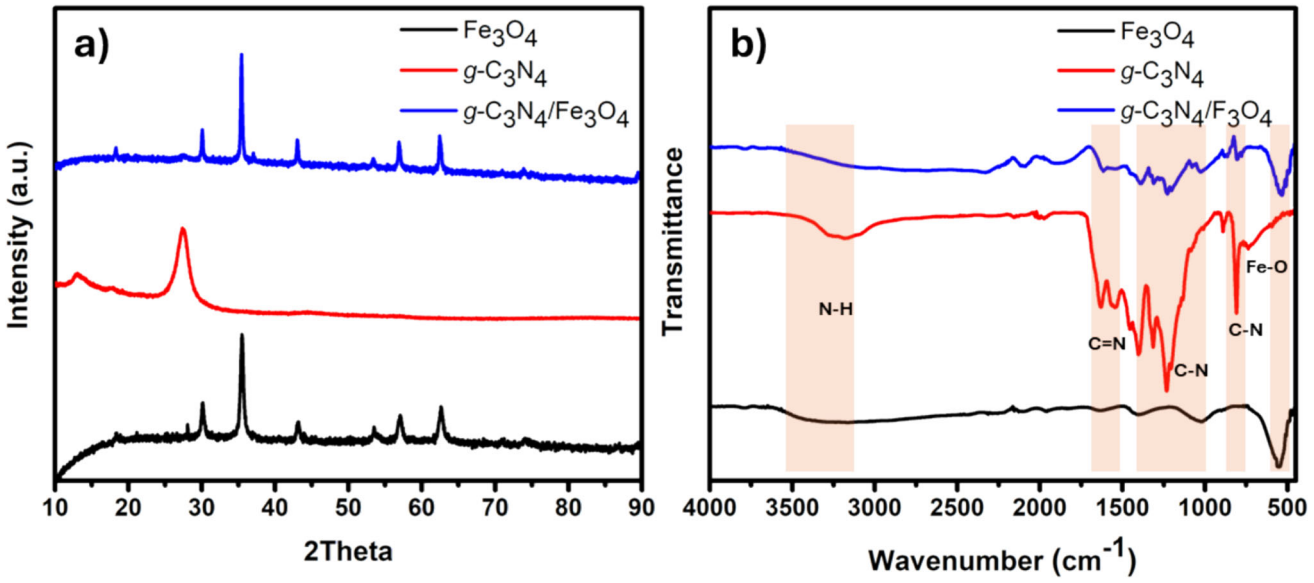

Fig. 1 **a** XRD patterns of Fe_3O_4 NPs, g-C_3N_4, NPs, and g-C_3N_4 @Fe_3O_4 NPs.**b** FTIR spectra of Fe_3O_4 NPs, g-C_3N_4 NPs, and g-C_3N_4 @Fe_3O_4 NPs.

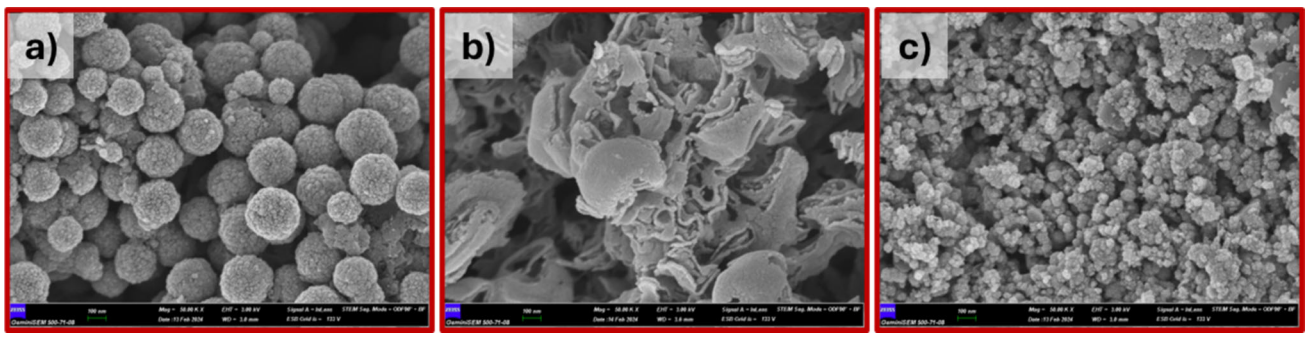

Fig. 2 **a** SEM image of Fe_3O_4 NPs (scale bar: 100 nm).**b** SEM image of g-C_3N_4 NPs (scale bar: 1 μm). **c** SEM image of g-C_3N_4 @Fe_3O_4 NPs (scale bar: 100 nm).

0.000874, and 0.01761 min^{-1} for g-C_3N_4, Fe_3O_4 and g-C_3N_4@Fe_3O_4, respectively (Fig. S2). Then, according to the data obtained, the reusability of the reaction with the highest activity of 100 mg g-C_3N_4@Fe_3O_4 photocatalyst was investigated. The reusability studies were easily carried out thanks to the photocatalyst, which can be easily separated from the reaction due to its magnetic feature. In reusability studies, the photocatalyst was collected from the reaction medium with the help of a magnet and washed. After reusability in three cycles, the degradation value of the paint decreased to 38.46% (Fig. 5c). This is caused by the surface of the photocatalyst being heavily covered with dye molecules, thus poisoning the photo catalyst.

The most closely related situation to the photocatalytic activities of catalysts is their ability to absorb light. The peaks of the photocatalyst components in the broad UV-visible region between 400 and 700 nm give the g-C_3N_4@Fe_3O_4 photocatalyst a broad absorption region. In this way, the use of light can be maximized and with more efficient light, more charge carriers are created and catalytic activity is increased. g-C_3N_4 NPs, one of the components of the photocatalyst, are the most effective material in collecting UV light and the excitation of electrons from the valence band to the conduction band. Fe_3O_4 plays an active role in the separation of charge carriers. In general, g-C_3N_4 can produce electron-hole pairs by excitation from light. Since the conduction band of g-C_3N_4 is more negatively charged than $O^2/\cdot O^{2-}$, it can reduce O^2 and release $\bullet O^{2-}$ radical to the environment [59]. Hydroxyl radical (·OH) are produced when water molecules (H_2O) react with holes in the valence band of g-C_3N_4. At this time, the holes in the CB of g-C_3N_4 will be transferred to the surface of Fe_3O_4, and electrons from g-C_3N_4 will be captured by Fe^{3+} to form Fe^{2+} (Fig. 6). All radicals formed reacts with BB3 dye and cause its degradation [36].

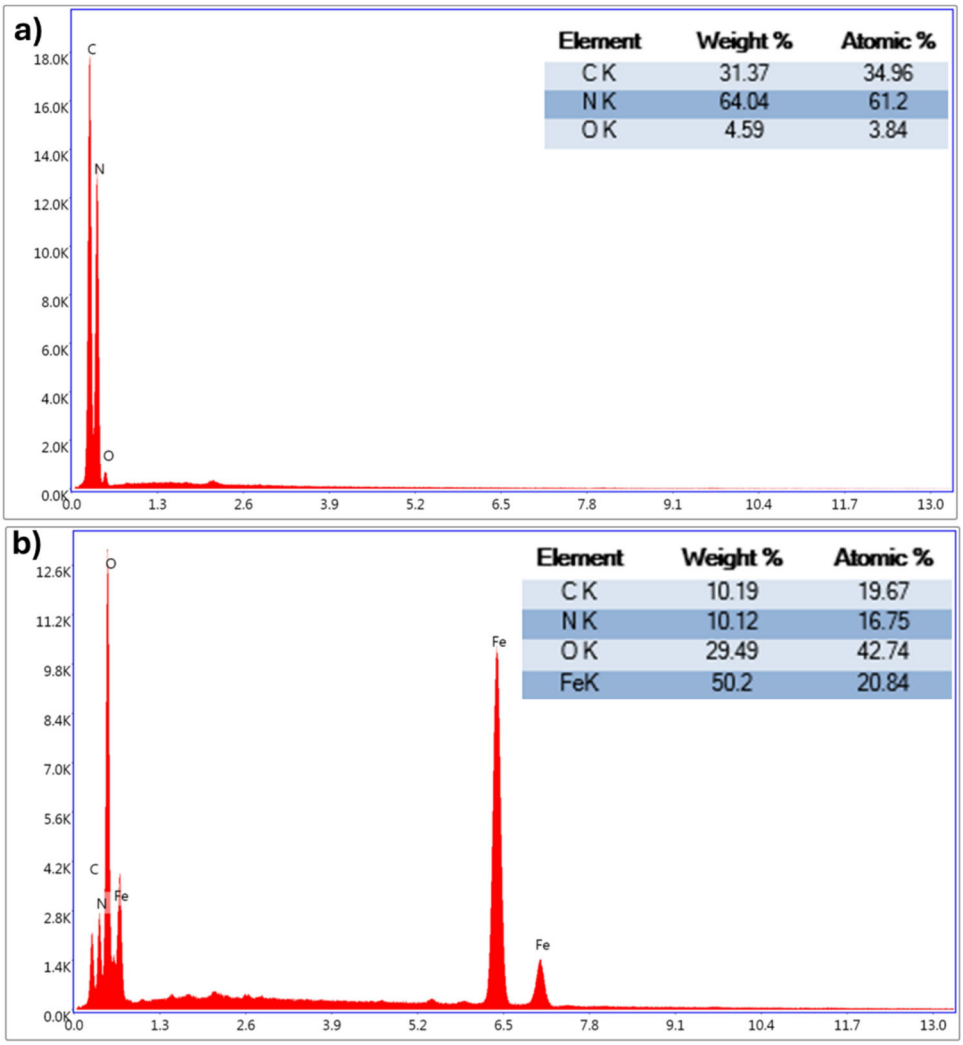

Fig. 3 EDX spectra of **a** g-C_3N_4 NPs, and **b** g-C_3N_4 @Fe_3O_4 NPs

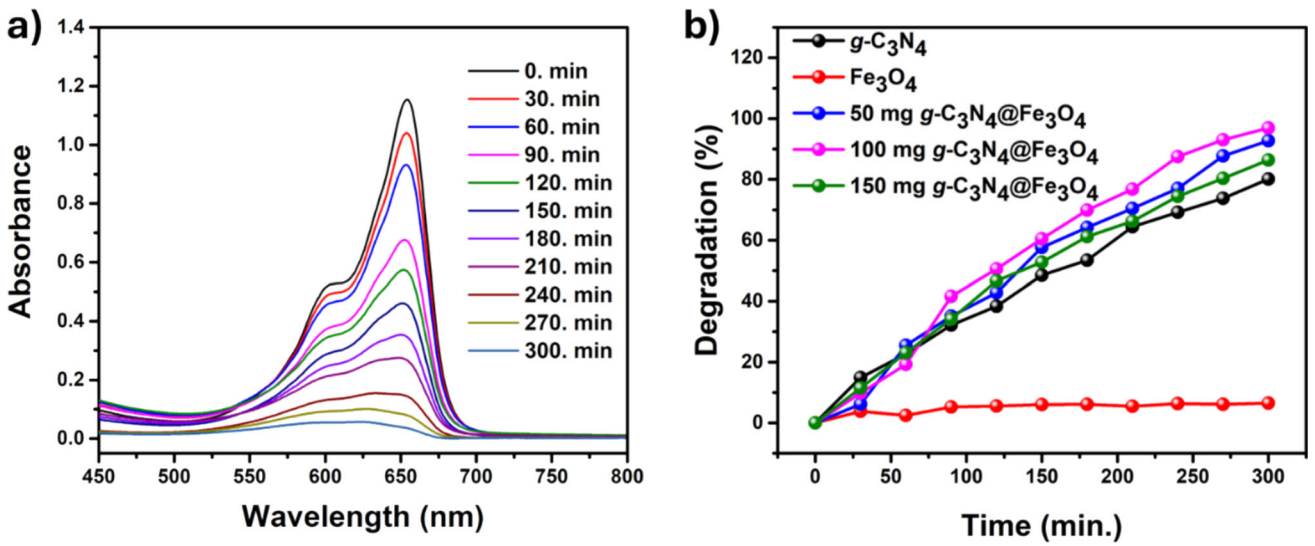

Fig. 4 **a** UV–Vis spectrum of the degradation of aqueous BB3 dye in the presence of 100 mg g-C_3N_4 @Fe_3O_4 nanocomposite at a duration interval ranging from 0 to 300 min.**b** Comparison of the percentage (%) photocatalytic degradation performance of Fe_3O_4, g-C_3N_4, and g-C_3N_4@Fe_3O_4 nanocomposite at different material amounts.

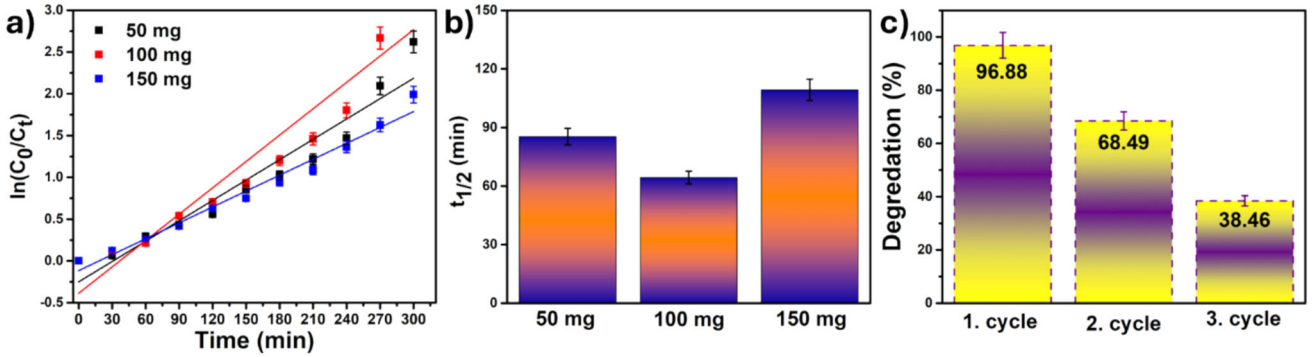

Fig. 5 **a** Photocatalytic activity of g-C_3N_4@Fe_3O_4 photocatalyst as a function of time. **b** Half-life time of the photocatalytic degradation rate of BB3 dye. **c** Reusability of g-C_3N_4@Fe_3O_4 photocatalyst 3 times in 300 min. of reaction

Fig. 7 Influence of pH on the extraction of BB3 dye ($n = 3$; last volume: 1.0mL, g-C_3N_4@Fe_3O_4 amount: 10 mg, adsorption duration: 3 min., desorption duration: 4 min)

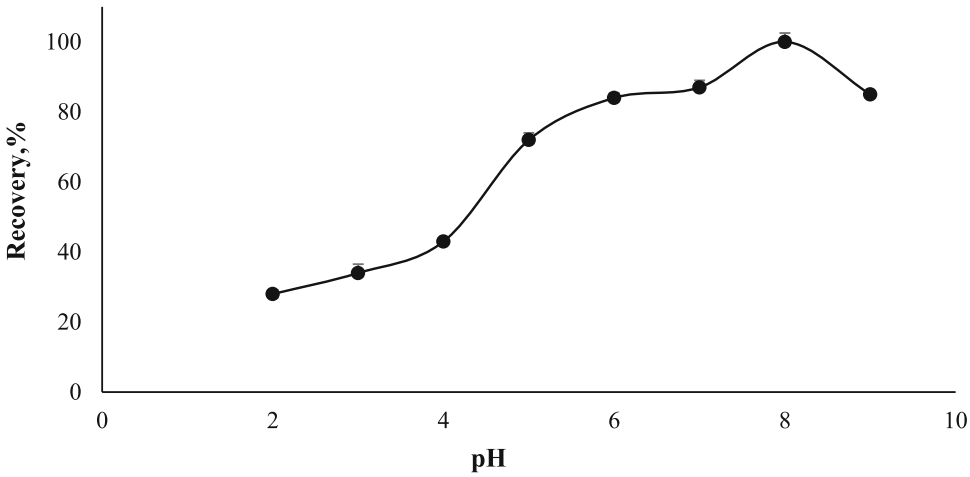

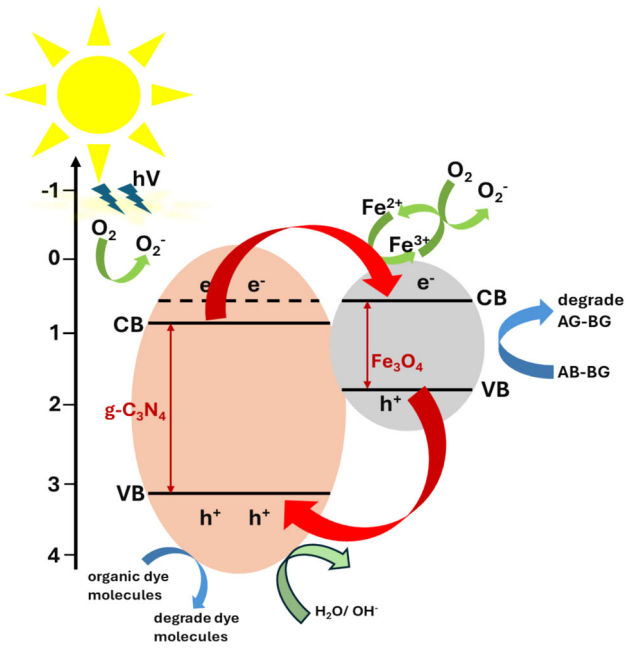

Fig. 6 Possible photocatalytic degradation mechanism of organic dye molecules in g-C_3N_4@Fe_3O_4 NPs [29, 36]

3.3 The g-C_3N_4@Fe_3O_4 Based MSPE Procedure Optimization

3.3.1 The Role of pH in the Extraction Efficiency of BB3 Dye

To begin with, it was comprehensively investigated whether pH affects the extraction efficiency of BB3 dye. The MSPE method was employed on model solutions adjusted to pH values between 2 and 9 with the use of buffer solutions. It can be seen from Fig. 7 that BB3 dye recoveries were not quantitative until pH 8, yet the best results were gained at pH 8. The pH of the solution generally affects the surface charge of the adsorbent (g-C_3N_4@Fe_3O_4) and the ionization state of the BB3 dye. Because of the adsorbent surface becomes negatively charged and BB3 dye molecules remain positively charged at pH 8, strong electrostatic attraction occurs between the BB3 cations and the negatively charged sites on the g-C_3N_4@Fe_3O_4 adsorbent. Therefore, the π–π stacking and hydrogen bonding between the BB3 dye and the g-C_3N_4-based adsorbent explain the high adsorption efficiency observed at pH 8 [60–62]. Similarly, lower extraction efficiency at acidic pHs (pHs < 4) could be associated with protonated groups. So, ongoing experiments were carried out

at this pH value in which BB3 dye was totally in its molecular form.

3.3.2 Assessment of the Effect of Extraction Duration on the Extraction Efficiency of BB3 Dye

Extraction time is the most vital parameter in MSPE techniques on account of the interaction between the analyte and adsorbent. For this purpose, the adsorption and desorption time should be researched if a developed microextraction method is MSPE. These processes were carried out by using an ultrasound stirring technique.

Firstly, model solutions were mixed as ultrasound in the range of 1–5 min, adsorption time in order to determine optimal value. The highest recoveries were obtained when the adsorption process was completed at 3 min. Similarly, desorption time was studied between 1 and 5 min with ultrasound mixers. The ultrasound technique ensured a recovery rate of more than 95% at the fourth. Both techniques' results were shown in Fig. 8. It was understood that the extraction would take place in a brief time with the help of an ultrasound system.

3.3.3 A Study on the Relationship Between Sample Volume and the Extraction Efficiency of BB3 dye

It is essential to investigate this parameter to calculate the preconcentration factor (PF) and establish the maximum allowable sample volume. Hence, the MSPE method was drawn on to the sample solutions prepared in the volume range of 5–40 mL. After, the final solutions were analyzed to check indigo carmines' absorbance values. As 95% recoveries went on stable for all samples, the sample volumes have been increased. Quantitative values for extraction of BB3 dye could be obtained up to 35 mL sample volume. That's why, it was considered that the MSPE method would be viable up to this maximum volume. The preconcentration factor was determined to be 35 (Fig. 9).

3.3.4 The Impact of Matrix Interferences on the BB3 Dye Extraction Efficiency

The foreign ions such as dyes and inorganic species [63, 64] can lead to inaccurate and non-selective results during extraction of BB3. Therefore, the influence of matrix components must be investigated by calculating their tolerance concentrations. In this method, some dyes and metals such as Red GRL, Red V.3R, Basic Yellow 28, Ponceau 4R, Azorubin, Brilliant Blue FCF, Indigo Carmine, Al^{3+}, Cu^{2+}, Ni^{2+}, and Na^{+} have been searched to create the best-analyzing environment for BB3 dye. Because of this, increasing amounts of matrix components were added to the real samples and then, the developed method was applied to them. The final ethanol phases were analyzed using a UV–Vis spectrophotometer, and the quantitative results shown in Table 1 demonstrate the good selectivity achieved by the MSPE method.

Table 1 The influence of organic and inorganic species on the extraction efficiency of BB3 dye (pH:8, $n = 3$, last volume: 1.0 mL, g-C_3N_4@Fe_3O_4 amount: 10 mg, adsorption duration: 3 min, desorption duration: 4 min)

Matrix ingredients	Concentration, μg L^{-1}	Recovery, %
Ponso 4R	604	98 ± 0[a]
Azorubine	502	100 ± 2
Indigo carmine	466	93 ± 5
Red GRL	433	100 ± 4
Brillant blue FCF	793	100 ± 0
Red V 3R	580	94 ± 4
Basic yellow 28	217	101 ± 5
Al^{3+}	1000	92 ± 1
Cu^{2+}	1000	96 ± 6
Ni^{2+}	1000	98 ± 3
Na^{+}	20000	94 ± 1

[a]Mean ± standard deviations

Table 2 The analysis of water samples (pH:8, $n = 3$, last volume: 1.0 mL, g-C_3N_4@Fe_3O_4 amount: 10 mg, adsorption duration: 3 min, desorption duration: 4 min)

Water samples	Added (μg mL^{-1})	Found (μg mL^{-1})	Recovery (%)
Wastewater 1	0.00	1.91 ± 0.00[a]	–
	0.50	2.40 ± 0.12	98
	1.00	2.87 ± 0.00	96
Wastewater 2	0.00	ND	–
	0.50	0.45 ± 0.01	90
	1.00	0.94 ± 0.00	94
Tap water	0.00	ND[a]	–
	0.50	0.50 ± 0.03	100
	1.00	0.91 ± 0.00	91

[a]Mean ± standard deviations, [b]*ND* Not detected

3.3.5 Applications

The optimized MSPE method has been implemented to textile and wastewater samples to analyze BB3 dye. Initially, the samples prepared as described in Sect. 2.5 were directly extracted without the addition of any analyte. BB3 dye was then added to these samples at concentrations ranging from 0.5 to 1.0 μg mL^{-1} to confirm the accuracy of the method. Table 2 illustrates that the standard addition method was

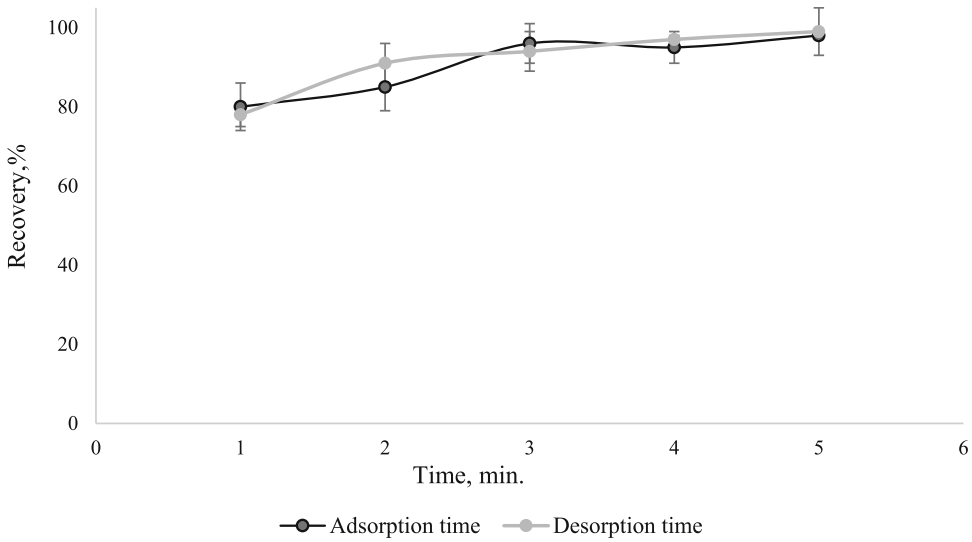

Fig. 8 Influence of extraction time on the extraction of BB3 dye (pH:8, $n = 3$, last volume: 1.0 mL, g-C_3N_4@Fe_3O_4 amount: 10 mg)

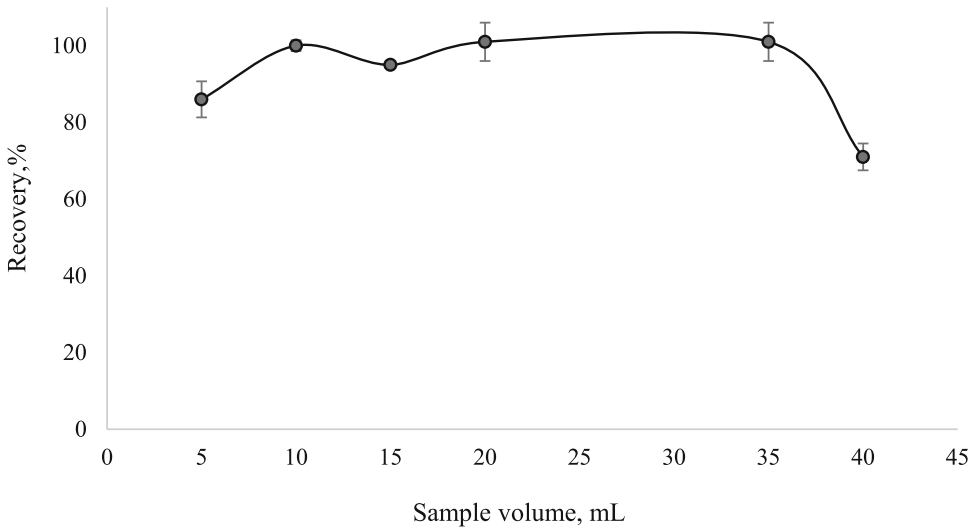

Fig. 9 Influence of sample volume on the extraction of BB3 dye (pH=8, $n = 3$; last volume: 1.0mL, g-C_3N_4@Fe_3O_4 amount: 10 mg, adsorption duration: 3 min, desorption duration: 4 min)

effectively implemented to quantify BB3 dye in textile samples. Furthermore, recoveries of BB3 dye from waste waters of up to 91% were achieved. In view of the fact that the results were quantitative, it was concluded that the MSPE method was accurate and was applicable. Finally, using the method applied directly to the fiber sample, its concentration was found to be 5.94 mg/kg.

3.3.6 Evaluation of the MSPE Method's Analytical Performance

The enhanced method was assessed under optimum conditions by determining some crucial parameters such as precision, limit of detection (LOD), limit of quantification (LOQ), correlation coefficient (R^2). The formulas for LOD, LOQ, and RSD are given by $3S_b/m$, $10S_b/m$, and S_b/x, respectively, where S_b represents the standard deviation, x is the concentration, and m is the slope. Thanks to six parallel blank solution measurements, LOD and LOQ was calculated to be 1.29 and 4.28 μg L^{-1}. On the other hand, R^2 was determined as 0.9976. The RSD, determined from five parallel measurements at the same concentration of the analyte, was calculated as 1.9. Finally, the linear calibration equation established was $A = 0.209C + 0.0327$, where A denotes absorbance and C signifies dye concentration. The g-C_3N_4@Fe_3O_4 hybrid material could be reused at a recovery rate of 81% until the fourth adsorption–desorption studies for BB3 extraction. Adsorption capacity of g-C_3N_4@Fe_3O_4 was also found as 285.5 mg g^{-1}.

On the other hand, Table 3 compares studies utilizing various photocatalytic reaction mechanisms to remove BB3 organic dye molecules. The synthesized g-C_3N_4@Fe_3O_4 was used for the adsorption and photocatalytic degradation of BB3, and 10 ppm of BB3 organic dye was degraded almost completely (96.8%) within 300 min, respectively. The materials used in the literature are examined, and it is

Table 3 Comparison of several studies using different composites in the removal of organic dyes (photocatalysis)

Photocatalyst	Dye concentration (mg/L)	Time (min)	Amount of photocatalyst (g/L)	Photocatalyst percentage (%)	Number of cycles	References
TiO_2	100	90	0.51	88.78	1	[8]
Sn-doped ZnS NPs	10	360	0.3	95	2	[65]
TiO_2 (Millennium PC-500 (size 5–10 nm) immobilized on non-woven paper)	10	120	Sludge covering 15 cm x 90 cm opening	71	1	[66]
TiO_2 (Millennium PC-500 (crystallite mean size 8 nm and surface area of 320.76 m^2/g) immobilized on glass plates)	10	200	0.264	63.36	1	[67]
$g\text{-}C_3N_4@Fe_3O_4$	10	300	0.1	96.8	3	This work

understood that they are used in only one method, while the $g\text{-}C_3N_4@Fe_3O_4$ hybrid material can be used in both magnetic solid-phase extraction (MSPE) and photocatalytic removal of BB3 dye. This is one of the most important advantages compared to other studies in the literature.

4 Conclusions

In this study, the effect of successfully synthesized $g\text{-}C_3N_4@Fe_3O_4$ nanomaterial on the MSPE of BB3 dye and photocatalytic wastewater removal efficiency was investigated. The removal study of this dye was carried out with $g\text{-}C_3N_4$, Fe_3O_4 and $g\text{-}C_3N_4@Fe_3O_4$ nanomaterials, respectively. The results show that an outstanding photocatalytic activity of 96.8% for 100 mg in 300 min was obtained in the study with $g\text{-}C_3N_4@Fe_3O_4$. This performance highlights the combined effect between $g\text{-}C_3N_4$ and Fe_3O_4, enhancing both the adsorption capacity and photocatalytic efficiency of the nanocomposite material. The performance of Fe_3O_4, which only achieved 6.5% degradation, was significantly improved when mixed with $g\text{-}C_3N_4$. This positions $g\text{-}C_3N_4@Fe_3O_4$ as a viable option for applications in environmental remediation. On the contrary, reusability studies revealed a decrease in the degradation efficiency of $g\text{-}C_3N_4@Fe_3O_4$ over multiple cycles. Therefore, further research is required to improve the long-term use stability of the material. The $g\text{-}C_3N_4@Fe_3O_4$ nanomaterial was used in the MSPE method performed in order to separate and also preconcentrate. The BB3 dye in wastewater and textile samples. The method has been successfully applied to these samples, demonstrating its versatility. Finally, the MSPE method was shown to be reliable and accurate for analytical purposes in validation studies using addition/recovery experiments with low LOD (1.29 $\mu g\ L^{-1}$), LOQ (4.28 $\mu g\ L^{-1}$) values and high recoveries between 91 and 100%. This research integrates the MSPE extraction method with photocatalytic degradation and presents an effective and low-cost strategy for the efficient removal of both organic and inorganic pollutants from wastewater, thereby contributing to sustainable environmental management and the protection of water quality. So this study will provide useful information for future water treatment studies.

Supplementary Information The online version contains supplementary material available at https://doi.org/10.1007/s13369-025-10937-w.

Acknowledgments The authors are grateful for the financial support of the Unit of the Scientific Research Projects of Erciyes University.

Data Availability Datasets of selected element concentrations were added as supplementary information.

Declarations

Competing interests The authors declare no competing interests.

Ethical Approval The work on this manuscript met all ethical standards required for research publication. No experiments with animals were performed.

Consent to Participate Human beings were not studied in this work.

Consent for Publication All authors will fully took part in this study, contributed to its content, and were informed on the progress of manuscript preparation.

References

1. Benkhaya, S.; M'rabet, S.; El Harfi, A.: A review on classifications, recent synthesis and applications of textile dyes. Inorg.

Chem. Commun. **115**, 107891 (2020). https://doi.org/10.1016/j.inoche.2020.107891
2. Manzoor, J.; Sharma, M.: Impact of textile dyes on human health and environment. IGI Global 162-169 (2020). https://doi.org/10.4018/978-1-7998-0311-9.ch008
3. Arora, S.: Textile Dyes: It's impact on environment and its treatment. J. Bioremed. Biodegrad. **5**(3) (2014). https://doi.org/10.4172/2155-6199.1000e146
4. Ozalp, O.; Soylak, M.: Microextraction methods for the separation-preconcentration and determination of food dyes: a minireview. Anal. Lett. **56**, 2473–2490 (2023). https://doi.org/10.1080/00032719.2023.2175212
5. Rehman, A.; Usman, M.; Bokhari, T.H.; ul Haq, A.; Saeed, M.; Rahman, H.M.A.U.; Siddiq, M.; Rasheed, A.; Nisa, M.U.: The application of cationic-nonionic mixed micellar media for enhanced solubilization of direct brown 2 dye. J. Mol. Liq. **301**, 112408 (2020). https://doi.org/10.1016/j.molliq.2019.112408
6. Belpaire, C.; Reyns, T.; Geeraerts, C.; Loco, J.V.: Toxic textile dyes accumulate in wild European eel Anguilla Anguilla. Chemosphere **138**, 784–791 (2015). https://doi.org/10.1016/j.chemosphere.2015.08.007
7. Li, P.; Zhao, J.; Zhai, X.; Wang, X.; Wen, Y.; Wu, L.: Liquid metal-embedded magnetic hydrogel beads as novel adsorbents for malachite green removal. Food Chem. **464**, 141842 (2025). https://doi.org/10.1016/j.foodchem.2024.141842
8. Buyukada, M.: Prediction of photocatalytic degradation and mineralization efficiencies of basic blue 3 using TiO_2 by nonlinear modeling based on Box-Behnken design. Arab. J. Sci. Eng. **41**, 2631–2646 (2016). https://doi.org/10.1007/s13369-016-2175-6
9. Alam, S.; Badshah, I.; Khan, S.; Shah, L.; Zahoor, M.; Umar, M.N., et al.: Synthesis and characterization of copper nanoparticle-based hydrogel and its applications in catalytic reduction and adsorption of basic blue 3. Heliyon (2024). https://doi.org/10.1016/j.heliyon.2024.e25836
10. Setiadi, T.; Andriani, Y.; Erlania, M.: Treatment of textile wastewater by a combination of anaerobic and aerobic processes: a denim processing plant case. Southeast Asian Water Environ. **1**, 159–166 (2006). https://www.researchgate.net/publication/342916898
11. Sharma, J.; Sharma, S.; Soni, V.: Classification and impact of synthetic textile dyes on aquatic flora: a review. Reg. Stud. Mar. Sci. **45**, 101802 (2021). https://doi.org/10.1016/j.rsma.2021.101802
12. Hu, B.; Hu, Q.; Hu, J.; Chen, C.: High-efficient capture of CI Basic Blue 3 by carboxymethyl-β-cyclodextrin conjugated magnetic composite. Desalin. Water Treat. **77**, 377–386 (2017). https://doi.org/10.5004/dwt.2017.20836
13. Khataee, A.R.; Fathinia, M.; Naseri, A.; Hasanzadeh, A.; Vafaei, F.; Emami, A., et al.: Modeling and optimization of simultaneous photocatalysis of three dyes on ceramic-coated TiO_2 nanoparticles using chemometrics methods: phytotoxicological assessment during degradation process. Res. Chem. Intermed. **40**, 1283–1302 (2014). https://doi.org/10.1007/s11164-013-1038-y
14. Sharma, K.; Sharma, P.; Dhiman, S.K.; Chadha, P.; Saini, H.S.: Biochemical genotoxic histological and ultrastructural effects on liver and gills of fresh water fish *Channa punctatus* exposed to textile industry intermediate 2 ABS. Chemosphere **287**, 132103 (2022). https://doi.org/10.1016/j.chemosphere.2021.132103
15. Singh, K.; Arora, S.: Removal of synthetic textile dyes from wastewaters: a critical review on present treatment technologies. Crit. Rev. Environ. Sci. Technol. **41**(9), 807–878 (2011). https://doi.org/10.1080/10643380903218376
16. Orts, F.; del Río, A.I.; Molina, J.; Bonastre, J.; Cases, F.: Electrochemical treatment of real textile wastewater: Trichromy Procion HEXL®. J. Electroanal. Chem. **808**, 387–394 (2018). https://doi.org/10.1016/j.jelechem.2017.06.051
17. Kariyajjanavar, P.; Jogttappa, N.; Nayaka, Y.A.: Studies on degradation of reactive textile dyes solution by electrochemical method. J. Hazard. Mater. **190**, 952–961 (2011). https://doi.org/10.1016/j.jhazmat.2011.04.032
18. Zubair, M.; Mu'azu, N.D.; Jarrah, N.; Blaisi, N.I.; Aziz, H.A.; Al-Harthi, M.A.: Adsorption behavior and mechanism of methylene blue, crystal violet, eriochrome black T, and methyl orange dyes onto biochar-derived date palm fronds waste produced at different pyrolysis conditions. Water Air Soil Pollut. **231**, 240 (2020). https://doi.org/10.1007/s11270-020-04595-x
19. Anouzla, A.; Abrouki, Y.; Souabi, S.; Safi, M.; Rhbal, H.: Colour and COD removal of disperse dye solution by a novel coagulant: application of statistical design for the optimization and regression analysis. J. Hazard. Mater. **166**, 1302–1306 (2009). https://doi.org/10.1016/j.jhazmat.2008.12.039
20. Soylak, M.; Ozalp, O.; Uzcan, F.: Magnetic nanomaterials for the removal, separation and preconcentration of organic and inorganic pollutants at trace levels and their practical applications: a review. Trends Environ. Anal. Chem. **29**, e00109 (2021). https://doi.org/10.1016/j.teac.2020.e00109
21. Jadhav, A.C.; Jadhav, N.C.: Treatment of textile wastewater using adsorption and adsorbents. In: Sustainable technologies for textile wastewater treatments. Woodhead Publishing, Sawston, pp 235–273 (2021). https://doi.org/10.1016/B978-0-323-85829-8.00008-0
22. Erdem, E.; Çölgeçen, G.; Donat, R.: The removal of textile dyes by diatomite earth. J. Colloid Interface Sci. **282**, 314–319 (2005). https://doi.org/10.1016/j.jcis.2004.08.166
23. Yuan, Y.; Wu, X.; Kalleshappa, B.; Pumera, M.: Light-programmable g-C_3N_4 microrobots with negative photogravitaxis for photocatalytic antibiotic degradation. Research **8**, 0565 (2025). https://doi.org/10.34133/research.0565
24. Liu, H.; Li, Y.; Xiang, Y.; Cao, H.; Li, Y.: Simultaneous determination of trace matrine and oxymatrine pesticide residues in tea by magnetic solid-phase extraction coupled with liquid chromatography-tandem mass spectrometry. J. Anal. Test. **8**(2), 245–250 (2024). https://doi.org/10.1007/s41664-024-00300-7
25. Chen, L.; Maigbay, M.A.; Li, M.; Qiu, X.: Synthesis and modification strategies of g-C_3N_4 nanosheets for photocatalytic applications. Adv. Powder Mater. **3**(1), 100150 (2024). https://doi.org/10.1016/j.apmate.2023.100150
26. Guo, X.; Duan, J.; Wang, W.; Zhang, Z.: Modified graphitic carbon nitride as the photocatalyst for wastewater treatment under visible light irradiation. Fuel **280**, 118544 (2020). https://doi.org/10.1016/j.fuel.2020.118544
27. Kadam, A.N.; Moniruzzaman, M.; Lee, S.W.: Dual functional S-doped g-C_3N_4 pinhole porous nanosheets for selective fluorescence sensing of Ag^+ and visible-light photocatalysis of dyes. Molecules **24**(3), 450 (2019). https://doi.org/10.3390/molecules24030450
28. Doan, A.T.; Phuc, N.V.; Tri, N.N.; Phu, H.T.; Hung, N.P.; Vien, V.: Sulfur-doped g-C_3N_4 with enhanced visible-light photocatalytic activity. Appl. Mech. Mater. **889**, 43–50 (2019). https://doi.org/10.4028/www.scientific.net/AMM.889
29. Zhang, Y.; Gong, H.; Li, G.; Zeng, H.; Zhong, L.; Liu, K.; Cao, H.; Yan, H.: Synthesis of graphitic carbon nitride by heating mixture of urea and thiourea for enhanced photocatalytic H_2 production from water under visible light. Int. J. Hydrogen Energy **42**, 143–151 (2016). https://doi.org/10.1016/j.ijhydene.2016.11.040
30. Dariani, R.S.; Esmaeili, A.; Mortezaali, A.; Dehghanpour, S.: Photocatalytic reaction and degradation of methylene blue on TiO_2 nano-sized particles. Optik **127**, 7143–7154 (2016). https://doi.org/10.1016/j.ijleo.2016.04.026
31. Rahman, Q.I.; Ahmad, M.; Misra, S.K.; Lohani, M.: Effective photocatalytic degradation of rhodamine B dye by ZnO nanoparticles. Mater. Lett. **91**(15), 170–174 (2013). https://doi.org/10.1016/j.matlet.2012.09.044
32. Houas, A.; Lachheb, H.; Ksibi, M.; Elaloui, E.; Guillard, C.; Herrmann, J.M.: Photocatalytic degradation pathway of methylene

blue in water. Appl. Catal. B Environ. **31**(2), 145–157 (2001). https://doi.org/10.1016/S0926-3373(00)00276-9
33. Batra, V.; Kaur, I.; Pathania, D.; Chaudhary, S.V.: Efficient dye degradation strategies using green synthesized ZnO-based nanoplatforms: a review. Appl. Surf. Sci. Adv. **11**, 100314 (2022). https://doi.org/10.1016/j.apsadv.2022.100314
34. Chen, D.; Cheng, Y.; Zhou, N.; Chen, P.; Wang, Y.; Li, K., et al.: Photocatalytic degradation of organic pollutants using TiO_2-based photocatalysts: a review. J. Clean. Prod. **268**, 121725 (2020). https://doi.org/10.1016/j.jclepro.2020.121725
35. Ani, I.J.; Akpan, U.G.; Olutoye, M.A.; Hameed, B.H.: Photocatalytic degradation of pollutants in petroleum refinery wastewater by TiO_2- and ZnO-based photocatalysts: recent development. J. Clean. Prod. **205**, 930–954 (2018). https://doi.org/10.1016/j.jclepro.2018.08.189
36. Sarp, G.; Yilmaz, E.: g-C_3N_4@ TiO_2@ Fe_3O_4 multifunctional nanomaterial for magnetic solid-phase extraction and photocatalytic degradation-based removal of trimethoprim and isoniazid. ACS Omega **7**(27), 23223–23233 (2022). https://doi.org/10.1021/acsomega.2c01311
37. Fu, J.; Yu, J.; Jiang, C.; Cheng, B.: G-C3N4-based heterostructured photocatalysts. Adv. Energy Mater. **8**, 314–319 (2018). https://doi.org/10.1002/aenm.201701503
38. Chalasani, R.; Vasudevan, S.: Cyclodextrin-functionalized Fe_3O_4@ TiO_2: reusable magnetic nanoparticles for photocatalytic degradation of endocrine-disrupting chemicals in water supplies. ACS Nano **7**, 4093–4104 (2013). https://doi.org/10.1021/nn400287k
39. Rodríguez-Ramos, R.; Socas-Rodríguez, B.; Santana-Mayora, Á.; Rodríguez-Delgado, M.Á.: Nanomaterials as alternative dispersants for the multiresidue analysis of phthalates in soil samples using matrix solid phase dispersion prior to ultra-high performance liquid chromatography tandem mass spectrometry. Chemosphere **236**, 124377 (2019). https://doi.org/10.1016/j.chemosphere.2019.124377
40. Zhang, Y.; Li, G.; Wu, D.; Li, X.; Yu, Y., et al.: Recent advances in emerging nanomaterials based food sample pretreatment methods for food safety screening. TrAC Trends Anal. Chem. **121**, 115669 (2019). https://doi.org/10.1016/j.trac.2019.115669
41. Sepehrmansourie, H.; Alamgholiloo, H.; Pesyan, N.N.; Zolfigol, M.A.: A MOF-on-MOF strategy to construct double Z-scheme heterojunction for high-performance photocatalytic degradation. Appl. Catal. B Environ. **321**, 122082 (2023). https://doi.org/10.1016/j.apcatb.2022.122082
42. Hunge, Y.M.; Yadav, A.A.; Khan, S.; Takagi, K.; Suzuki, N.; Teshima, K., et al.: Photocatalytic degradation of bisphenol A using titanium dioxide@nanodiamond composites under UV light illumination. J. Colloid Interface Sci. **582**, 1058–1066 (2021). https://doi.org/10.1016/j.jcis.2020.08.102
43. Xia, S.; Zhang, L.; Pan, G.; Qian, P.; Ni, Z.: Photocatalytic degradation of methylene blue with a nanocomposite system: synthesis, photocatalysis and degradation pathways. Phys. Chem. Chem. Phys. **17**, 5345–5351 (2015). https://doi.org/10.1039/C4CP03877K
44. Ighnih, H.; Haounati, R.; Malekshah, R.E.; Ouachtak, H.; Jada, A.; Addi, A.A.: Photocatalytic degradation of RhB dye using hybrid nanocomposite BiOCl@Kaol under sunlight irradiation. J. Water Process Eng. **54**, 103925 (2023). https://doi.org/10.1016/j.jwpe.2023.103925
45. Trinh, D.T.T.; Channei, D.; Nakaruk, A.; Khanitchaidecha, W.: New insight into the photocatalytic degradation of organic pollutant over $BiVO_4$/SiO_2/GO nanocomposite. Sci. Rep. **11**, 4620 (2021). https://doi.org/10.1038/s41598-021-84323-5
46. Nivetha, M.R.S.; Kumar, J.V.; Ajarem, J.S.; Allam, A.A.; Manikandan, V.; Arulmozhi, R., et al.: Construction of SnO_2/g-C_3N_4 an effective nanocomposite for photocatalytic degradation of amoxicillin and pharmaceutical effluent. Environ. Res. **209**, 112809 (2022). https://doi.org/10.1016/j.envres.2022.112809
47. Zhao, X.; Qu, S.; Han, J.: Photocatalytic degradation of tetracycline on g-C_3N_4@ Fe_3O_4 magnetic photocatalyst. Desalin. Water Treat. **150**, 213–219 (2019). https://doi.org/10.5004/dwt.2019.23621
48. Wei, X.N.; Wang, H.L.: Preparation of magnetic g-C_3N4/Fe_3O_4/TiO_2 photocatalyst for visible light photocatalytic application. J. Alloys Compd. **763**, 844–853 (2018). https://doi.org/10.1016/j.jallcom.2018.06.031
49. Ceylan, A.; Karagoz, S.; Tekin, S.; Kayaci, N.; Pekdemir, S.; Salem, S., et al.: TiO_2 and Ag NPs modified polyacrylonitrile NFs: antimicrobial, self-cleaning and SERS sensing capabilities for protective clothing applications. Colloids Surf. A Physicochem. Eng. Asp. **678**, 132432 (2023). https://doi.org/10.1016/j.colsurfa.2023.132432
50. Yilmaz, E.; Salem, S.; Sarp, G.; Aydin, S.; Sahin, K.; Korkmaz, I.; Yuvali, D.: TiO_2 nanoparticles and C-Nanofibers modified magnetic Fe_3O_4 nanospheres (TiO_2@Fe_3O_4@C–NF): a multifunctional hybrid material for magnetic solid-phase extraction of ibuprofen and photocatalytic degradation of drug molecules and azo dye. Talanta **213**, 120813 (2020). https://doi.org/10.1016/j.talanta.2020.120813
51. Karagoz, S.; Kiremitler, N.B.; Sakir, M.; Salem, S.; Onses, M.S.; Sahmetlioglu, E.; Ceylan, A.; Yilmaz, E.: Synthesis of Ag and TiO_2 modified polycaprolactone electrospun nanofibers (PCL/TiO_2-Ag NFs) as a multifunctional material for SERS, photocatalysis and antibacterial applications. Ecotoxicol. Environ. Saf. **188**, 109856 (2020). https://doi.org/10.1016/j.ecoenv.2019.109856
52. Kizil, N.; Erbilgin, D.; Basaran, E.; Yola, M.L.; Yilmaz, E.; Marouch, S.; Soylak, M.: Determination of Rhodamine B in cosmetics, candy, water, and plastic by a novel multiwalled carbon nanotube (MWCNT)@Zinc Oxide@Magnetite nanocomposite for magnetic solid-phase extraction (MSPE) with spectrophotometric detection. Anal. Lett. **57**, 1182–1196 (2023). https://doi.org/10.1080/00032719.2023.2243353
53. Ge, L.: Synthesis and photocatalytic performance of novel metal-free g-C_3N_4 photocatalysts. Mater. Lett. **65**, 2652–2654 (2011). https://doi.org/10.1016/j.matlet.2011.05.069
54. Liu, J.; Zhang, T.; Wang, Z.; Dawson, G.; Chen, W.: Simple pyrolysis of urea into graphitic carbon nitride with recyclable adsorption and photocatalytic activity. J. Mater. Chem. **21**, 14398–14401 (2011). https://doi.org/10.1039/C1JM12620B
55. He, W.; Jia, H.; Li, Z.; Miao, C.; Lu, R.; Zhang, S.; Zhang, Z.: Magnetic recyclable g-C_3N_4/Fe_3O_4@MIL-100(Fe) ternary catalyst for photo-Fenton degradation of ciprofloxacin. J. Environ. Chem. Eng. **10**, 108698 (2022). https://doi.org/10.1016/j.jece.2022.108698
56. Ali, A.; Amin, M.; Tahir, M.; Ali, S.S.; Hussain, A.; Ahmad, I.; Mahmood, A.; Farooq, M.U.; Farid, M.A.: g-C_3N_4/Fe_3O_4 composites synthesized via solid-state reaction and photocatalytic activity evaluation of methyl blue degradation under visible light irradiation. Front. Mater. **10**, 1180646 (2023). https://doi.org/10.3389/fmats.2023.1180646
57. Sohrabi, M.R.; Ghavami, M.: Photocatalytic degradation of Direct Red 23 dye using UV/TiO_2: effect of operational parameters. J. Hazard. Mater. **153**, 1235–1239 (2008). https://doi.org/10.1016/j.jhazmat.2007.09.114
58. Kaneco, S.; Rahman, M.A.; Suzuki, T.; Katsumata, H.; Kiyohisa, O.: Optimization of solar photocatalytic degradation conditions of bisphenol A in water using titanium dioxide. J. Photochem. Photobiol. A Chem. **163**, 419–424 (2004). https://doi.org/10.1016/j.jphotochem.2004.01.012
59. Habibi-Yangjeh, A.; Asadzadeh-Khaneghah, S.; Feizpoor, S.; Rouhi, A.: Review on heterogeneous photocatalytic disinfection of waterborne, airborne, and foodborne viruses: can we win against

pathogenic viruses? J. Colloid Interface Sci. **580**, 503–514 (2020). https://doi.org/10.1016/j.jcis.2020.07.047
60. Zhang, Y.; Liu, H.; Xu, B.: Adsorption of Basic Blue 3 onto magnetic nanocomposite adsorbents: effect of pH and mechanism analysis. J. Mol. Liq. **335**, 116212 (2021). https://doi.org/10.1016/j.molliq.2021.116212
61. Wang, X.; Li, J.; Chen, Z.; Zhao, Y.: Magnetic g-C_3N_4/Fe_3O_4 nanocomposite for efficient removal of cationic dyes: effect of surface charge and pHpzc. Appl. Surf. Sci. **475**, 1–10 (2019). https://doi.org/10.1016/j.apsusc.2019.01.042
62. Li, Q.; Wang, Z.; Gao, L.: π–π stacking and hydrogen-bond interactions in dye adsorption on g-C_3N_4-based magnetic composites. Colloids Surf. A Physicochem. Eng. Asp. **600**, 124920 (2020). https://doi.org/10.1016/j.colsurfa.2020.124920
63. Erbas, Z.; Soylak, M.: Determination of Rhodamine B in water and cosmetics by switchable solvent-based liquid phase microextraction with spectrophotometric determination. Instrum. Sci. Technol. **51**, 290–302 (2023). https://doi.org/10.1080/10739149.2022.2127109
64. El-Rayyes, A.; Mortada, W.I.: Micelle-mediated extraction combined with the adsorption onto magnetic nanoparticles for the extraction of crystal violet from wastewater. Bull. Chem. Soc. Ethiop. **39**, 425–435 (2025). https://doi.org/10.4314/bcse.v39i3.3
65. Shah, U.; Jan, F.A.; Ullah, R.; Ullah, W.N.; Ahmad, M.: Photocatalytic degradation of acidic and basic dye by ZnS and tin-doped ZnS nanocatalysts. Iran. J. Sci. **47**(3), 733–747 (2023). https://doi.org/10.1007/s40995-023-01462-2
66. Khataee, A.R.; Fathinia, M.; Aber, S.; Zarei, M.: Optimization of photocatalytic treatment of dye solution on supported TiO_2 nanoparticles by central composite design: intermediates identification. J. Hazard. Mater. **181**, 886–897 (2010). https://doi.org/10.1016/j.jhazmat.2010.05.096
67. Fathinia, M.; Khataee, A.R.; Zarei, M.; Aber, S.: Comparative photocatalytic degradation of two dyes on immobilized TiO_2 nanoparticles: effect of dye molecular structure and response surface approach. J. Mol. Catal. A Chem. **333**, 73–84 (2010). https://doi.org/10.1016/j.molcata.2010.09.018